

Exact nonstationary solutions to the mean-field equations of motion for two-component Bose-Einstein condensates in periodic potentials

R. Mark Bradley

Department of Physics, Colorado State University, Fort Collins, CO 80523 USA

Bernard Deconinck and J. Nathan Kutz

*Department of Applied Mathematics,
University of Washington, Seattle, WA 98195 USA*

Abstract

We study the dynamics of two-component Bose-Einstein condensates in periodic potentials in one dimension. Elliptic potentials which have the sinusoidal optical potential as a special case are considered. We construct exact nonstationary solutions to the mean-field equations of motion. Among the solutions are two types of temporally-periodic solutions — in one type there are condensate oscillations between neighboring potential wells, while in the other the condensates oscillate from side to side within the wells. Our numerical studies of the stability of these solutions suggests the existence of one-parameter families of stable nonstationary solutions.

I. Introduction

In conventional magnetic traps, the spins of the alkali atoms making up a Bose-Einstein condensate (BEC) are frozen, and all atoms are in the first hyperfine manifold. Thus, even if the atoms have spin, the condensate order parameter ψ is a single complex scalar.

Over the last few years, two methods to produce mixtures of two distinguishable BEC's have been developed and implemented. In these condensate mixtures, ψ has two components. The Boulder group, for example, produced a mixture of two condensates consisting of two different hyperfine spin states of ^{87}Rb [1, 2]. Initially, a single condensate in the spin state $|1\rangle$ with hyperfine spin $F = 1$ was trapped magnetically. A two-photon transition was then used to transfer a portion of the atoms to a second spin state $|2\rangle$ with $F = 2$. Once the two-photon pulse had ended, the number of atoms in each condensate was essentially constant. Modugno *et al.* [3], on the other hand, produced a mixture of two Bose-Einstein condensates of different atomic species, ^{41}K and ^{87}Rb [4].

An atom placed in a standing light wave is subject to induced dipole forces. The resulting atomic potential is sinusoidal, and is referred to as an optical lattice. Merely by altering the phase, wavelength and intensity of the light, the position, lattice spacing and well depth of the optical lattice can be adjusted. Thus, optical lattices are well-characterized and controllable.

By adiabatically increasing the depth of the lattice potential, trapped BEC's can be transferred into an optical lattice. BEC's on optical lattices have attracted a great deal of interest for several reasons. In experiments, the analogs of the ac and dc Josephson effects [5], Bloch oscillations and Landau-Zener tunneling [6], number-squeezed states [7], and the Mott-insulator transition [8] have been studied. In addition, an optical lattice in which each site is occupied by a single alkali atom in its ground state is a promising candidate for a register in a quantum computer. One route currently being explored to initialize such a register is to begin with a BEC and then adiabatically turn on an optical lattice, with the result that one atom in its ground state occupies each site [9]. From a theoretical standpoint, BEC's on optical lattices are interesting because the simple sinusoidal form of the potential has made it possible to obtain some exact solutions to the mean-field equations of motion, in spite of their nonlinearity [10, 11, 12, 13].

Two condensates confined to a cigar-shaped trap are quasi-one-dimensional if the trap is highly elongated and if the transverse dimensions of the trap are comparable to the healing

lengths. A quasi-one-dimensional optical lattice can be realized by superimposing a standing light wave on the cigar-shaped trap. In the mean-field approximation, the condensates are described by coupled nonlinear Schrödinger equations in one space dimension with periodic external potentials.

In this paper, we study the dynamics of two-component condensates in periodic potentials in one dimension (1D). We will consider elliptic potentials which have the sinusoidal potential as a special case. Exact stationary solutions to this problem have been found by Deconinck *et al.* [12]. We will use these solutions to construct exact *nonstationary* solutions to the problem. Our numerical studies of the stability of these solutions strongly suggest that there are one-parameter families of stable solutions.

We will only study condensate mixtures in which the atoms of the different components have the same atomic mass μ . This means that mixtures of condensates of different atomic species are excluded from our analysis, and accordingly we will confine ourselves to consideration of the two-component condensates like those studied by the Boulder group [1, 2].

The paper is organized as follows. In Section II, we introduce the mean-field equations of motion and develop a general method of constructing nonstationary solutions. This method is applied to condensates in a 1D elliptic potential in Sec. III, and the physical interpretation of the resulting solutions is discussed in Sec. IV. The stability of the solutions is the subject of Sec. V. Finally, we summarize our results in Sec. VI.

II. General Development

In the two-component condensates studied by the Boulder group, the number of atoms in each condensate is nearly constant [1, 2]. We will therefore neglect loss of atoms to the normal phases and switching of atoms from one condensate to another. The mean-field equations of motion are then

$$i\hbar \frac{\partial \psi_j}{\partial t} = -\frac{\hbar^2}{2\mu} \frac{\partial^2 \psi_j}{\partial x^2} + \left(\sum_{l=1}^2 \alpha_{jl} |\psi_l|^2 \right) \psi_j + V_j \psi_j \quad (1)$$

for $j = 1, 2$. Here $\psi_j = \psi_j(x, t)$ is the condensate wave function for the j th species and α_{jl} describes the interaction of an atom in the j th condensate and an atom in the l th condensate. The 2×2 symmetric matrix $M = \{\alpha_{ij}\}$ will be referred to as the interaction matrix. The interaction strengths α_{11} , α_{12} and α_{22} are known to the 1% level for ^{87}Rb , and are in the proportion 1.02 : 1 : 0.97 [14]. We shall neglect the difference between the interaction strengths and set $\alpha = \alpha_{11} = \alpha_{12} = \alpha_{22}$.

In the case of an optical lattice, the potentials V_1 and V_2 are sinusoidal. V_1 and V_2 are very nearly equal for linearly polarized light, provided that the detuning is not too small [15]. We shall neglect the difference $V_1 - V_2$ and set

$$V \equiv V_1 = V_2 = -V_0 \sin^2 qx, \quad (2)$$

where V_0 is a constant which depends on the intensity of the light, $q \equiv 2\pi/\lambda$ and λ is the optical wavelength. In fact, we will study the more general potential

$$V = -V_0 \text{sn}^2(qx, k), \quad (3)$$

where $\text{sn}(qx, k)$ is the Jacobian elliptic sine function with elliptic modulus $k \in [0, 1]$. The potential (3) reduces to the optical potential (2) for $k = 0$ and to the single potential well (or barrier) $V = -V_0 \tanh^2 qx$ for $k = 1$. For $0 < k < 1$, the potential is periodic with period $2K(k)/q$, where

$$K(k) \equiv \int_0^{\pi/2} \frac{d\theta}{\sqrt{1 - k^2 \sin^2 \theta}}. \quad (4)$$

Plots of the potential (3) for a range of k values may be found in Ref. [10]. To simplify the notation, we will not display the k dependence of the Jacobian elliptic functions from this point on.

Let $\vec{\psi} \equiv (\psi_1, \psi_2)^T$. With the simplifications we have made, the equation of motion is

$$i\hbar \frac{\partial \vec{\psi}}{\partial t} = -\frac{\hbar^2}{2\mu} \frac{\partial^2 \vec{\psi}}{\partial x^2} + \alpha(\vec{\psi}^\dagger \vec{\psi})\vec{\psi} - V_0 \text{sn}^2(qx) \vec{\psi}. \quad (5)$$

This equation is further simplified by introducing the dimensionless variables $\tilde{x} = qx$, $\tilde{t} = \hbar q^2 t / \mu$, $\tilde{\psi}_j = (\sqrt{|\alpha|\mu}/\hbar q)\psi_j$, $\tilde{\alpha} = \text{sgn}(\alpha)$ and $\tilde{V}_0 = \mu V_0 / (\hbar q)^2$ and then dropping the tildes.

This gives

$$i \frac{\partial \vec{\psi}}{\partial t} = -\frac{1}{2} \frac{\partial^2 \vec{\psi}}{\partial x^2} + \alpha(\vec{\psi}^\dagger \vec{\psi})\vec{\psi} - V_0 \text{sn}^2(x) \vec{\psi}. \quad (6)$$

If U is a 2×2 unitary matrix,

$$\vec{\psi}' \equiv U \vec{\psi} \quad (7)$$

is also a solution to the equation of motion (6) [16]. This observation will allow us to construct nonstationary solutions from the stationary solutions of Deconinck *et al.* [17].

III. Construction of the Nonstationary Solutions

Nonstationary solutions can be constructed for both $\alpha = +1$ and $\alpha = -1$. For $\alpha = -1$, any two atoms attract each other, regardless of whether or not they belong to the same

condensate. Thus, the nonstationary solutions are likely unstable against collapse for $\alpha = -1$. We will therefore restrict our attention to the case $\alpha = +1$ for the remainder of the paper.

Let A and B be arbitrary nonnegative real numbers. From Ref. [12] we obtain three types of stationary solutions to Eq. (6):

Type I with

$$\vec{\psi} = \begin{pmatrix} A \operatorname{cn} x \\ B \operatorname{dn} x e^{i(1-k^2)t/2} \end{pmatrix} \exp \left[-i \left(\frac{1}{2} + A^2 + B^2 \right) t \right] \quad (8)$$

and

$$V = (k^2 + A^2 + k^2 B^2) \operatorname{sn}^2 x; \quad (9)$$

Type II with

$$\vec{\psi} = \begin{pmatrix} A \operatorname{sn} x \\ B \operatorname{dn} x e^{it/2} \end{pmatrix} \exp \left\{ -i \left[\frac{1}{2} (1 + k^2) + A^2 + B^2 \right] t \right\} \quad (10)$$

and

$$V = (k^2 - A^2 + k^2 B^2) \operatorname{sn}^2 x + A^2; \quad (11)$$

and lastly Type III with

$$\vec{\psi} = \begin{pmatrix} A \operatorname{sn} x \\ k B \operatorname{cn} x e^{ik^2 t/2} \end{pmatrix} \exp \left\{ -i \left[\frac{1}{2} (1 + k^2) + A^2 + k^2 B^2 \right] t \right\} \quad (12)$$

and

$$V = (k^2 - A^2 + k^2 B^2) \operatorname{sn}^2 x + A^2. \quad (13)$$

We now apply a unitary transformation to these solutions: we set $\vec{\psi}' = U(\theta) \vec{\psi}$, where

$$U(\theta) = \begin{pmatrix} \cos \theta & \sin \theta \\ -\sin \theta & \cos \theta \end{pmatrix}. \quad (14)$$

Formally, we can think of $\vec{\psi}$ as being the wave function of a spin-1/2 particle. $U(\theta)$ then represents a rotation in spin space through an angle $\beta = -2\theta$ about the y -axis. The external potential is unchanged by the transformation [18].

We may confine our attention to the interval $0 \leq \theta < \pi$ because $U(\pi) \vec{\psi}' = -\vec{\psi}'$. In fact, it is possible to reduce this interval. To see this, let $\vec{\Psi}(x, t; \theta) = \vec{\psi}'(x, t)$ and note that $\vec{\Psi}(x, t; \theta + \pi/2) = U(\pi/2) \vec{\Psi}(x, t; \theta) = (\vec{\Psi}_2(x, t; \theta), -\vec{\Psi}_1(x, t; \theta))^T$. Now if $(\psi_1, \psi_2)^T$ is a

solution to the equation of motion (6), then so is $(e^{i\phi_1}\psi_1, e^{i\phi_2}\psi_2)^T$ for arbitrary real constants ϕ_1 and ϕ_2 . Moreover, these solutions have the same physical meaning. Apart from a switch in the labels 1 and 2 and an irrelevant phase change, therefore, $\vec{\Psi}(x, t; \theta + \pi/2)$ and $\vec{\Psi}(x, t; \theta)$ are identical, and it suffices to consider the interval $0 \leq \theta \leq \pi/2$. There is a symmetry about $\theta = \pi/4$ that enables us to further pare down the range of θ we must consider. We begin with the observation that

$$U\left(\frac{\pi}{2} - \theta\right) = \begin{pmatrix} 0 & 1 \\ 1 & 0 \end{pmatrix} U(\theta) \begin{pmatrix} -1 & 0 \\ 0 & 1 \end{pmatrix}. \quad (15)$$

For Types I, II and III, $\vec{\psi}$ has the form $(f_1(x)e^{-i\omega_1 t}, f_2(x)e^{-i\omega_2 t})^T$. Employing the identity (15), we obtain

$$\vec{\Psi}\left(x, t; \frac{\pi}{2} - \theta\right) = \exp\left[-i\pi\left(\frac{\omega_2}{\omega_2 - \omega_1}\right)\right] \begin{pmatrix} 0 & 1 \\ 1 & 0 \end{pmatrix} \vec{\Psi}\left(x, t - \frac{\pi}{\omega_1 - \omega_2}; \theta\right). \quad (16)$$

This means that except for a switch in the labels 1 and 2 and an irrelevant phase factor, $\vec{\Psi}(x, t; \frac{\pi}{2} - \theta)$ and $\vec{\Psi}(x, t - \frac{\pi}{\omega_2 - \omega_1}; \theta)$ are the same. Thus, we need only consider the interval $0 \leq \theta \leq \pi/4$.

$\vec{\psi}' = U(\theta)\vec{\psi}$ is a nonstationary solution for $0 < \theta \leq \pi/4$ if $\vec{\psi}$ is a stationary solution of Type I, II or III. Other types of stationary solution are constructed in Ref. [12]: There are solutions in which both ψ_1 and ψ_2 are proportional to the same Jacobian elliptic function, as well as solutions in which $|\psi_i|^2$ is a linear function of a Jacobian elliptic function for $i = 1$ and 2. However, when a unitary transformation is applied to solutions of these types, the result is simply another stationary solution of the same kind. Therefore, we will not consider these solutions further.

IV. Physical Interpretation of the Nonstationary Solutions

A. The Trigonometric Limit $k = 0$

In the $k = 0$ limit, the Jacobian elliptic functions reduce to trigonometric functions. For solutions of Type I, the density of condensate 1 is

$$n'_1 \equiv |\psi'_1|^2 = A^2 \cos^2 \theta \cos^2 x + B^2 \sin^2 \theta + AB \sin 2\theta \cos x \cos(t/2), \quad (17)$$

while the density of condensate 2 is given by

$$n'_2 \equiv |\psi'_2|^2 = A^2 \sin^2 \theta \cos^2 x + B^2 \cos^2 \theta - AB \sin 2\theta \cos x \cos(t/2). \quad (18)$$

n'_1 and n'_2 oscillate in time with period $T = 4\pi$ (in unscaled physical units $T = 4\pi\mu/\hbar q^2$). The potential $V = A^2 \sin^2 x$ is an optical potential with minima at the points $x = m\pi$, where m is any integer. We divide the lattice of potential minima into two sublattices: sublattice 1 with even m , and sublattice 2 with odd m . The total condensate density $n' \equiv n'_1 + n'_2 = A^2 \cos^2 x + B^2$ is independent of time, and its maxima occur at the potential minima. At time $t = 0$, the global maxima of n'_1 are on sublattice 1, while at time $t = T/2$, they are on sublattice 2 (Fig. 1). Naturally, at time $t = T$, the global maxima of n'_1 have returned to sublattice 1. Note that the global maxima reside on one of the two sublattices for all times t , and their locations change discontinuously as time passes. The global maxima of n'_2 also oscillate between sublattices 1 and 2, but the oscillations of n'_2 lag those of n'_1 by half a period. When the condensates move between the two sublattices in this way, we will say that they undergo sublattice oscillations.

In the $k = 0$ limit, the solutions of Types I and II become identical, apart from a translation of both $\vec{\psi}'$ and V through $\pi/2$. The Type III solution reduces to a stationary solution already studied by Deconinck *et al.* [12] and will not be considered further here.

B. Solutions with $0 < k < 1$

We now turn to the nature of the solutions for $0 < k < 1$. Explicitly, the Type I solution is

$$\vec{\psi}' = \begin{pmatrix} A \cos \theta \text{cn} x + B \sin \theta \text{dn} x e^{i(1-k^2)t/2} \\ -A \sin \theta \text{cn} x + B \cos \theta \text{dn} x e^{i(1-k^2)t/2} \end{pmatrix} \exp \left[-i \left(\frac{1}{2} + A^2 + B^2 \right) t \right]. \quad (19)$$

The potential minima appear on the lattice of points $x = 2mK$, where m is any integer. We again divide the lattice of potential minima into two sublattices: sublattice 1 with even m , and sublattice 2 with odd m . The two condensates execute sublattice oscillations with temporal period $T = 4\pi/(1 - k^2)$, as shown in Fig. 2.

The nature of the solutions of Types II and III is more complex. We will continue to refer to the set of points $x = 2mK$ with integer m as the lattice, and to divide this lattice into sublattices 1 and 2. The potential minima are on the lattice for $0 \leq A < k\sqrt{1 + B^2}$. For $A > k\sqrt{1 + B^2}$, on the other hand, the potential maxima are on the lattice, and the minima lie on the set of points $x = lK$, where l is any odd integer.

Let $\langle n'_j \rangle$ be the temporal average of n'_j . For solutions of Types II and III, we say that the motion of condensate j is of type α (β) if the maxima of $\langle n'_j \rangle$ are located at the odd (even) multiples of K . The motion of the two condensates will be said to be of type $\gamma\delta$ if

the motion of condensate 1 is of type γ and the motion of condensate 2 is of type δ , where γ and δ can be either α or β .

We begin by considering the solutions of Type II. If the motion of condensate j is of type β , the maxima of n'_j smoothly oscillate from side to side as time passes and the oscillations of adjacent maxima in n'_j are 180° out of phase. Let $N_l^{(j)}$ be the number of atoms of species j on the interval $(l-1)K < x < (l+1)K$ for all odd integers l . If the motion of condensate j is of type α , then $N_{4m+1}^{(j)}$ oscillates periodically in time for each integer m . $N_{4m-1}^{(j)}$ also oscillates periodically in time, but the oscillations of $N_{4m-1}^{(j)}$ lag those of $N_{4m+1}^{(j)}$ by half a period. For motion of both types α and β , the period of the temporal oscillations T is 4π .

As shown in Fig. 3, motion of types $\alpha\alpha$, $\alpha\beta$, and $\beta\beta$ occurs for different ranges of the parameters θ and $A/(kB)$. (Motion of the type $\beta\alpha$ occurs in part of the region with $\pi/4 < \theta \leq \pi/2$; these solutions are mapped to the $\alpha\beta$ sector in the region with $0 \leq \theta < \pi/4$ by the symmetry transformation discussed in Sec. III.) In the $\beta\beta$ sector of the “phase diagram,” the maxima of both n'_1 and n'_2 reside in the potential wells. The maxima of n'_1 oscillate from side to side within the wells, and the oscillations of adjacent maxima are 180° out of phase (see Fig. 4). The maxima of n'_2 oscillate in the same fashion, but the temporal oscillations of n'_2 lag those of n'_1 by half a period.

If $A/(kB)$ is greater than both $\cot \theta$ and $\sqrt{1+B^{-2}}$, the motion is of type $\alpha\alpha$, and the potential minima are at the points $x = lK$, where l is odd. The number of atoms of condensate 1 in the potential well centered on the point $x = (4m+1)K$ (i. e., $N_{4m+1}^{(1)}$) oscillates periodically in time for each integer m . The number of atoms of condensate 1 in the potential well centered on the point $x = (4m-1)K$ (i. e., $N_{4m-1}^{(1)}$) also oscillates periodically in time, but the oscillations of $N_{4m-1}^{(1)}$ lag those of $N_{4m+1}^{(1)}$ by half a period. The motion of condensate 2 is analogous to that of condensate 1, except that it lags that of condensate 1 by half a period. Finally, the total condensate density $n' = n'_1 + n'_2$ depends on position but is independent of time.

For $k \leq 1/\sqrt{2}$, the motion just described is simply a sublattice oscillation, and the global maxima of n'_1 and n'_2 are always located at potential minima. A curious but interesting type of motion can occur for $k > 1/\sqrt{2}$, though. In this case, for certain values of the parameters, as a global maximum in n'_j grows in amplitude, it is initially located at the potential minimum. However, as its height continues to increase, the global maximum can split into two global maxima that are located to either side of the potential minimum (see

Fig. 5).

In the region of the phase diagram in which $1 < A/(kB) < \sqrt{1+B^{-2}}$ and $0 \leq \theta \leq \pi/4$, motion of types $\alpha\alpha$ and $\alpha\beta$ occurs, but the maxima of the total condensate density n' are located at *maxima* of the potential. These solutions are therefore expected to be unstable, and this is confirmed by our numerical simulations.

We now turn to the nature of the solutions of Type III. In motion of both types α and β , the maxima and minima of n'_j oscillate continuously from side to side, and all of maxima and minima remain in phase with one another. The phase diagram for the solutions of Type III is given by Fig. 3, just as it was for the solutions of Type II. In the region of the phase diagram in which $1 < A/(kB) < \sqrt{1+B^{-2}}$ and $0 \leq \theta \leq \pi/4$, the maxima of the total condensate density n' are located at maxima of the potential, and the solutions are expected to be unstable [19]. Outside this region, the maxima of n' coincide with the minima of the potential. If $A/(kB)$ is greater than both $\cot \theta$ and $\sqrt{1+B^{-2}}$, the motion is of the type $\alpha\alpha$ and the maxima of both n'_1 and n'_2 reside in the potential wells. The maxima of n'_1 oscillate continuously from side to side and in phase with one another (see Fig. 6). The oscillations of the two condensates are 180° out of phase, and, as a result, the total condensate density n' does not depend on time. Qualitatively speaking, the same type of intra-well oscillation occurs in the $\beta\beta$ sector of the phase diagram. The two condensates oscillate in phase with one another in the $\alpha\beta$ sector of the phase diagram, but the maxima of $\langle n'_1 \rangle$ coincide with the minima of $\langle n'_2 \rangle$. For all solutions of Type III, the period of oscillation $T = 4\pi/k^2$.

For solutions of both Types II and III, an interesting special case is obtained for $A/(kB) = \sqrt{1+B^{-2}}$. The external potential V is simply a constant in this case. Motion of type $\alpha\beta$ occurs if $\theta < \cot^{-1}(\sqrt{1+B^{-2}})$; otherwise, the motion is of type $\alpha\alpha$.

C. The Hyperbolic Limit $k = 1$

The Jacobian elliptic functions reduce to hyperbolic functions for $k = 1$. The Type I solution becomes a stationary solution studied in Ref. [12]. The Type II and III solutions, on the other hand, are identical for $k = 1$. Since these solutions are nonstationary, we will briefly consider their physical interpretation.

The external potential for Type II solutions is $V = (1 - A^2 + B^2) \tanh^2 x + A^2$. A method of producing a potential with a $\tanh^2 x$ spatial dependence in an experiment is yet to be found. The case $A = \sqrt{1+B^2}$ is therefore of particular interest, since V is simply a constant in that case. For $\cot^{-1}(\sqrt{1+B^{-2}}) < \theta < \pi/4$, a bound pair of dark solitons

oscillate about the origin. The two dark solitons move 180° out of phase with one another. For $0 < \theta < \cot^{-1}(\sqrt{1+B^{-2}})$, on the other hand, a dark soliton and a bright soliton oscillate in phase about the origin. The bright soliton cannot exist in isolation since the atoms repel one another, but the presence of the dark soliton stabilizes the bright soliton. Both of these kinds of solution — oscillating dark-dark and dark-bright soliton pairs — have previously been found by Park and Shin [16].

This discussion suggests an alternative way of thinking about the special cases mentioned at the close of Section IV C. For both Types II and III, solutions of type $\alpha\beta$ have dark-bright soliton pairs oscillating about the lattice points, while solutions of type $\alpha\alpha$ have bound pairs of dark solitons oscillating about these points. The dark-bright pairs oscillate in phase with each other. In contrast, the oscillations of the pairs of dark solitons are 180° out of phase. Neighboring solitons in n'_j oscillate 180° out of phase in Type II solutions, whereas for Type III solutions neighboring solitons in n'_j oscillate in phase with one another.

V. Numerical Investigation of the Stability of the Nonstationary Solutions

$\vec{\psi}' = U(\theta)\vec{\psi}$ is a stable solution to the equation of motion (6) if and only if $\vec{\psi}$ is a stable solution to that equation. This observation has two notable consequences. First, analytical results on the stability of stationary solutions were obtained in Ref. [12] and $\vec{\psi}$ is a stationary solution. Unfortunately, these analytical results are of no use here, as they only apply if the interaction matrix M is nonsingular. We will therefore probe the stability of the nonstationary solutions numerically. Secondly, in our numerical work it is sufficient to investigate the stability of our solutions for a single value of θ , which we choose to be $\pi/4$.

Our numerical method consists of solving the equation of motion (6) using a fourth-order Runge-Kutta method in time with a filtered pseudo-spectral method in space. For each run, a small amount of white noise was added to the initial data and the time for the onset of instability t^* was determined. For all simulations,

$$t^* \equiv \min_{t>0} \left\{ t : \frac{|U_n(t) - U(t)|}{U_n(t) + U(t)} = 0.1 \right\},$$

where $U(t) \equiv \max_x \{|\psi'_1(x,t)|, |\psi'_2(x,t)|\}$, $U_n(t) \equiv \max_x \{|\psi'_{1n}(x,t)|, |\psi'_{2n}(x,t)|\}$, and ψ'_{1n} and ψ'_{2n} represent the first and second components of the numerical solutions for ψ'_1 and ψ'_2 , respectively.

The parameter space of our nonstationary solutions is too large to permit a comprehensive study of all possibilities. Instead, we will consider specific one-parameter families of

solutions, and determine how t^* varies as the parameter changes.

A. Trigonometric solutions close to the uniform solution

The class of solutions considered first is trigonometric, and hence $k = 0$. Setting $\theta = \pi/4$, $A = \sqrt{2}\epsilon$, $B = \sqrt{2}$ and changing the zero of energy, the solution of Type I becomes

$$\vec{\psi}' = \begin{pmatrix} 1 + \epsilon e^{-it/2} \cos x \\ 1 - \epsilon e^{-it/2} \cos x \end{pmatrix} \quad (20)$$

with

$$V = -2 - 2\epsilon \cos^2 x. \quad (21)$$

As the parameter $\epsilon \rightarrow 0$, this solution approaches the stationary uniform solution, which is known to be stable [12]. We investigated the stability of this class of solutions for a range of values of ϵ . In Fig. 7, t^* is plotted as a function of ϵ . The instability onset time t^* appears to diverge as ϵ approaches ϵ^c from above, where $\epsilon^c \approx 0.2$. Two numerical runs are not displayed in Fig. 7: we find that $t^*(\epsilon = 0.205) > 60000$ and $t^*(\epsilon = 0.2) > 132000$. These results strongly suggest that t^* is infinite for $\epsilon < \epsilon^c$, and hence that there is a one-parameter family of stable solutions given by Eq. (20) with $\epsilon < \epsilon^c \approx 0.2$.

The behavior of an unstable solution with $\epsilon = 1/2$ is illustrated in Fig. 8. For this value of ϵ , the solution is far from being uniform even at early times. After the onset of the instability at time $t^* \approx 450$, the solution loses much of its coherence, although some is retained and new, larger-scale structures develop, as seen in Figs. 8 (c) and (d).

B. Trigonometric solutions with increasing offset

The second class of solutions considered is also trigonometric. With $\theta = \pi/4$, $A = 1$, $B = \sqrt{-\frac{1}{2} - 2\epsilon}$ and $V = 2\epsilon + \frac{1}{2} - \cos^2 x$, the solution of Type I becomes

$$\vec{\psi}' = \begin{pmatrix} \sqrt{-\frac{1}{4} - \epsilon} + \frac{e^{-it/2}}{\sqrt{2}} \cos x \\ \sqrt{-\frac{1}{4} - \epsilon} - \frac{e^{-it/2}}{\sqrt{2}} \cos x \end{pmatrix}. \quad (22)$$

In general, we define the offset of a solution to be the smallest value that $\min[n'_1(x, t), n'_2(x, t)]$ takes on for all x and t . The offset of the solution (22) increases as $\epsilon \rightarrow -\infty$. It was shown in Ref. [12] that increased offset stabilizes some stationary solutions. This motivated us to consider the class of solutions (22) with increasingly more negative ϵ . In Fig. 9, the instability onset time t^* is shown for a range of ϵ values. t^* remains finite for $-\epsilon$ as large as 10, and it seems likely that t^* is finite for all $-\epsilon < \infty$. If this is indeed the case, the solutions (22) are all unstable.

C. A class of elliptic solutions

The third class of solutions we consider is not trigonometric, i. e., $k \neq 0$. In all numerical runs, $k = 0.999$, and so the solutions and the external potential are far from trigonometric. With $\theta = \pi/4$, $A = \epsilon$ and $B = 1 + \epsilon/k$, the solution of Type II is

$$\vec{\psi}' = \begin{pmatrix} \frac{\epsilon}{\sqrt{2}} e^{-i\omega_1 t} \text{sn} x + \frac{1}{\sqrt{2}} \left(1 + \frac{\epsilon}{k}\right) e^{-i\omega_2 t} \text{dn} x \\ -\frac{\epsilon}{\sqrt{2}} e^{-i\omega_1 t} \text{sn} x + \frac{1}{\sqrt{2}} \left(1 + \frac{\epsilon}{k}\right) e^{-i\omega_2 t} \text{dn} x \end{pmatrix}, \quad (23)$$

with $\omega_1 = (1 + k^2)/2 + (1 + \epsilon/k)^2$, $\omega_2 = k^2/2 + (1 + \epsilon/k)^2$, and an appropriate additive shift of the potential. As $\epsilon \rightarrow 0$, this solution approaches a stationary solution which has been proven to be linearly stable in the case of a nonsingular interaction matrix [12]. This motivates the consideration of the family of solutions (23) with parameter ϵ . In Fig. 10, the instability onset time t^* is shown for different values of ϵ . The behavior of t^* is quite interesting, as it displays one local maximum and one local minimum in the range of ϵ considered. It is possible other local extrema exist for values of $\epsilon > 1.5$, but solving the equation of motion numerically becomes progressively more difficult as ϵ increases because the nonlinearity grows stronger. As ϵ approaches $\epsilon^c \approx 0.375$ from above, t^* appears to diverge. Thus, there seems to be a whole band of stable nonstationary solutions with the stationary solution as a limiting case.

For values of $\epsilon > \epsilon^c$, the solution (23) is unstable, and interesting structures appear after the onset of the instability. Figs. 11 - 13 illustrate various aspects of this behavior for $k = 0.999$ and $\epsilon = 1/2$. From these figures, we see that the solution becomes unstable shortly before $t = 1640$, and then is modulated in time with a period long compared to that of the intra-well oscillations. The amplitude of the density oscillations within the potential wells varies by up to a factor of five. After about three periods of the modulation, the modulated state in turn becomes unstable shortly after time $t = 2600$.

These phenomena are also readily observed in the Fourier transform of the solution, which is shown in Fig. 13. Note the change in the spectrum during the modulated stage of the time evolution: the amplitudes of the Fourier coefficients change, but the number of activated modes remains approximately constant. The modulated state itself becomes unstable after a few periods of the modulation, and a band of approximately 60 unstable modes is excited, resulting in an apparent loss of coherence in the density.

VI. Summary

In this paper, we studied the dynamics of two-component Bose-Einstein condensates in periodic potentials in one dimension. Elliptic potentials which have the sinusoidal optical potential as a special case were considered. We constructed exact nonstationary solutions to the mean-field equations of motion by performing a unitary transformation on previously-known stationary solutions. Among the solutions are two types of temporally-periodic solutions — in one type of solution there are condensate oscillations between neighboring potential wells and in the other type the condensates oscillate from side to side within the wells. Our numerical studies of the stability of these solutions suggests the existence of one-parameter families of stable solutions for both sinusoidal optical potentials and for elliptic potentials.

R. M. B. thanks J. Roberts for useful discussions; B. D. and J. N. K. acknowledge support from the National Science Foundation (DMS-0139093 and DMS-0092682 respectively).

-
- [1] C. J. Myatt, E. A. Burt, R. W. Ghrist, E. A. Cornell, and C. E. Wieman, Phys. Rev. Lett. **78**, 586 (1997).
 - [2] D. S. Hall, M. R. Matthews, J. R. Ensher, C. E. Wieman, and E. A. Cornell, Phys. Rev. Lett. **81**, 1539 (1998).
 - [3] G. Modugno, M. Modugno, F. Riboli, G. Roati, and M. Inguscio, Phys. Rev. Lett. **89**, 190404 (2002).
 - [4] Optically-trapped condensates with $F = 1$ and $F = 2$ have also been produced. ψ has three components for the case $F = 1$ and five for $F = 2$. See D. M. Stamper-Kurn, M. R. Andrews, A. P. Chikkatur, S. Inouye, H.-J. Miesner, J. Stenger, and W. Ketterle, Phys. Rev. Lett. **80**, 2027 (1998); J. Stenger, S. Inouye, D. M. Stamper-Kurn, H.-J. Miesner, A. P. Chikkatur, and W. Ketterle, Nature **396**, 345 (1998); and H. Schmaljohann, M. Erhard, J. Kronjäger, M. Kottke, S. van Staa, L. Cacciapuoti, J. J. Arlt, K. Bongs, and K. Sengstock, Phys. Rev. Lett. **92**, 40402 (2004).
 - [5] B. P. Anderson and M. A. Kasevich, Science **282**, 1686 (1998); F. S. Cataliotti, S. Burger, C. Fort, P. Maddaloni, F. Minardi, A. Trombettoni, A. Smerzi, and M. Inguscio, *ibid* **293**, 843 (2001).
 - [6] O. Morsch, J. H. Müller, M. Cristiani, D. Ciampini, and E. Arimondo, Phys. Rev. Lett. **87**,

- 140402 (2001).
- [7] C. Orzel, A. K. Tuchman, M. L. Fenselau, M. Yasuda, and M. A. Kasevich, *Science* **291**, 2386 (2001).
 - [8] M. Greiner, O. Mandel, T. Esslinger, T. W. Hänsch, and I. Bloch, *Nature* **415**, 39 (2002).
 - [9] J. V. Porto, S. Rolston, B. Laburthe Tolra, C. J. Williams, and W. D. Phillips, *Phil. Trans. R. Soc. Lond. A* **361**, 1417 (2003).
 - [10] J. C. Bronski, L. D. Carr, B. Deconinck, J. N. Kutz, and K. Promislow, *Phys. Rev. E* **63**, 036612 (2001).
 - [11] J. C. Bronski, L. D. Carr, R. Carretero-González, B. Deconinck, J. N. Kutz, and K. Promislow, *Phys. Rev. E* **64**, 056615 (2001).
 - [12] B. Deconinck, J. N. Kutz, M. S. Patterson, and B. W. Warner, *J. Phys. A* **36**, 5431 (2003).
 - [13] B. Deconinck, B. A. Frigyik, and J. N. Kutz, *J. Nonlinear Sci.* **12**, 169 (2002).
 - [14] J. P. Burke, Jr., J. L. Bohn, B. D. Esry, and C. H. Greene, *Phys. Rev. A* **55**, 2511 (1997).
 - [15] J. Roberts, private communication.
 - [16] Unitary transformations of solutions to Eq. (6) in the absence of an external potential have already been studied: see Q. Han Park and H. J. Shin, *Phys. Rev. E* **61**, 3093 (2000).
 - [17] Very recently, a perturbative treatment in which the external potential and the nonlinear terms were treated as small was used to obtain nonstationary solutions to Eq. (6). See M. A. Porter, P. G. Kevrekidis and B. A. Malomed, [nlin.CD/0401023](#).
 - [18] $\vec{\psi}' = U(\theta)\vec{\psi}$ is not the most general unitary transformation, but the most general transformation only adds phase changes to $\vec{\psi}_1$ and $\vec{\psi}_2$ and a change in the zero of time.
 - [19] This expectation is borne out by our numerical integrations of the equations of motion.

Figure Captions

1. n'_1 (shown in dark gray) as a function of space and time in the optical potential (shown in light gray). The parameter values for this case are $k = 0$, $A = B = 1/\sqrt{2}$ and $\theta = \pi/8$. Note that the temporal oscillations of n'_2 lag those of n'_1 by half a period.

2. n'_1 for a solution of Type I as a function of space and time. The external potential V is shown at the rear of the figure. The parameter values for this case are $k = 0.99$, $A = B = 1/\sqrt{2}$ and $\theta = \pi/8$. As before, the temporal oscillations of n'_2 lag those of n'_1 by half a period.

3. A “phase diagram” showing the types of motion which occur for different values of the parameters θ and A/kB . This figure applies to solutions of both Types II and III. For $0 \leq A/kB < \sqrt{1 + B^{-2}}$, the potential minima are on the lattice of points $x = 2mK$, where m is an integer. For $A/kB > \sqrt{1 + B^{-2}}$, on the other hand, the potential maxima are on the lattice, and the minima lie on the set of points $x = lK$, where l is any odd integer.

4. n'_1 for a solution of Type II in the $\beta\beta$ sector of the phase diagram as a function of space and time. The external potential V is shown at the rear of the figure. The parameter values for this case are $k = 0.99$, $A = 1$, $B = 3$ and $\theta = \pi/4$. Note the oscillations of the condensate from side to side within the potential wells.

5. n'_1 for a solution of Type II in the $\alpha\alpha$ sector of the phase diagram as a function of space and time. The external potential V is shown at the rear of the figure. The parameter values for this case are $k = 0.99$, $A = 2.5$, $B = 1$ and $\theta = \pi/4$. Note the periodic splitting of the peaks in n'_1 as the overall amount of condensate 1 in the potential wells rises and falls.

6. n'_1 for a solution of Type III in the $\alpha\alpha$ sector of the phase diagram as a function of space and time. The external potential V is shown at the rear of the figure. The parameter values for this case are $k = 0.99$, $A = 3$, $B = 1$ and $\theta = \pi/8$.

7. The instability onset time t^* for the solutions given by Eq. (20). t^* appears to diverge as ϵ approaches $\epsilon^c \approx 0.2$ from above.

8. The onset of the instability for the trigonometric solution (20) with $\epsilon = 1/2$ in a computational domain of size $L = 8\pi$. Figures (a) and (b) show the density of the first and second condensate components, respectively. Figures (c) and (d) are the corresponding gray scale plots. Regions of high (low) density are shaded black (white).

9. The instability onset time t^* for the solutions given by Eq. (22).

10. The instability onset time t^* for the solutions given by Eq. (23). t^* appears to diverge

as ϵ approaches $\epsilon^c \approx 0.375$ from above.

11. The behavior of the elliptic solution (23) with $\epsilon = 1/2$, $k = 0.999$, $L = 16K(0.999)$ and $\xi = x + L/16$, immediately after the onset of the instability. Figures (a) and (b) show the densities of the first and second condensates, respectively. Figures (c) and (d) are the corresponding gray scale plots of these quantities.

12. The behavior of the elliptic solution (23) with $\epsilon = 1/2$, $k = 0.999$, $L = 16K(0.999)$ and $\xi = x + L/16$, from before the onset of the instability until well after the end of the modulated phase of the motion. The left and right figures are gray scale plots of the densities of the first and second condensates, respectively.

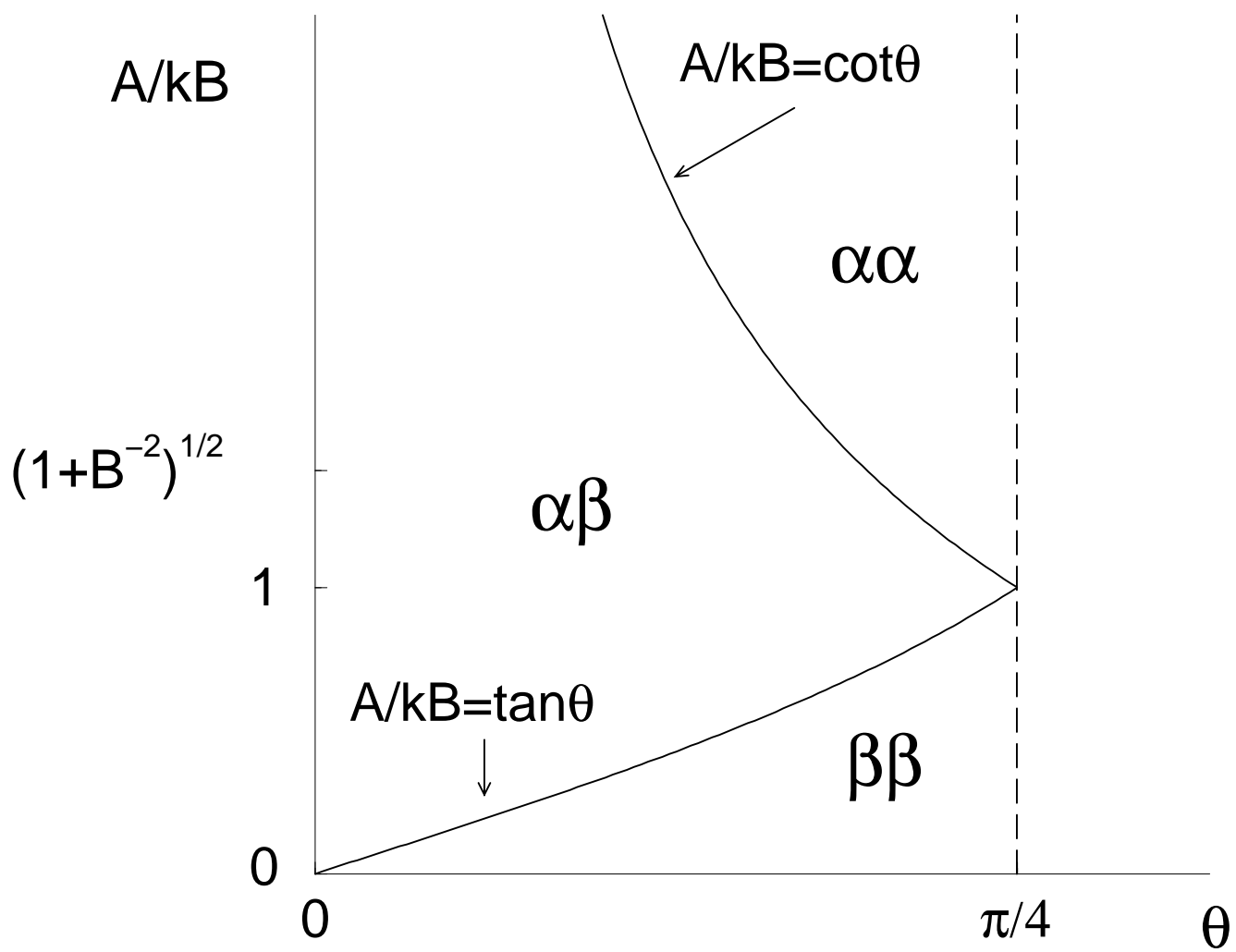
13. Numerical Fourier spectrum of the solution (23) with $\epsilon = 1/2$ and $k = 0.999$. Only 60 of the 512 modes used are shown. The left and right figures are the Fourier transforms of n'_1 and n'_2 , respectively.

This figure "figure1.gif" is available in "gif" format from:

<http://arXiv.org/ps/nlin/0403043v1>

This figure "figure2.gif" is available in "gif" format from:

<http://arXiv.org/ps/nlin/0403043v1>



This figure "figure4.gif" is available in "gif" format from:

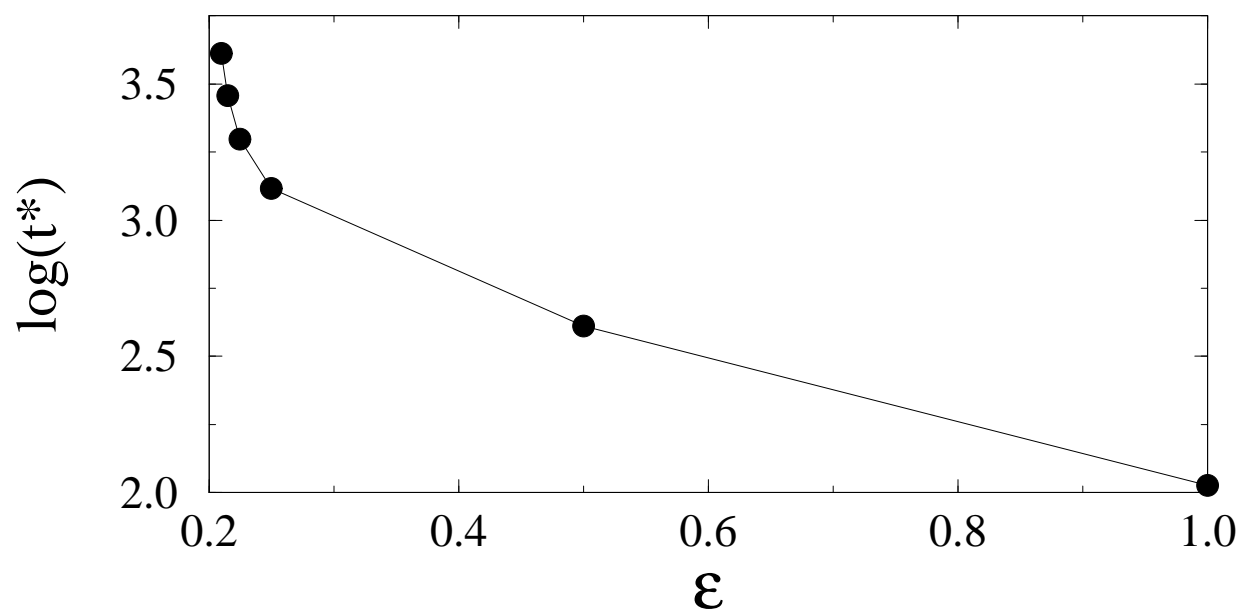
<http://arXiv.org/ps/nlin/0403043v1>

This figure "figure5.gif" is available in "gif" format from:

<http://arXiv.org/ps/nlin/0403043v1>

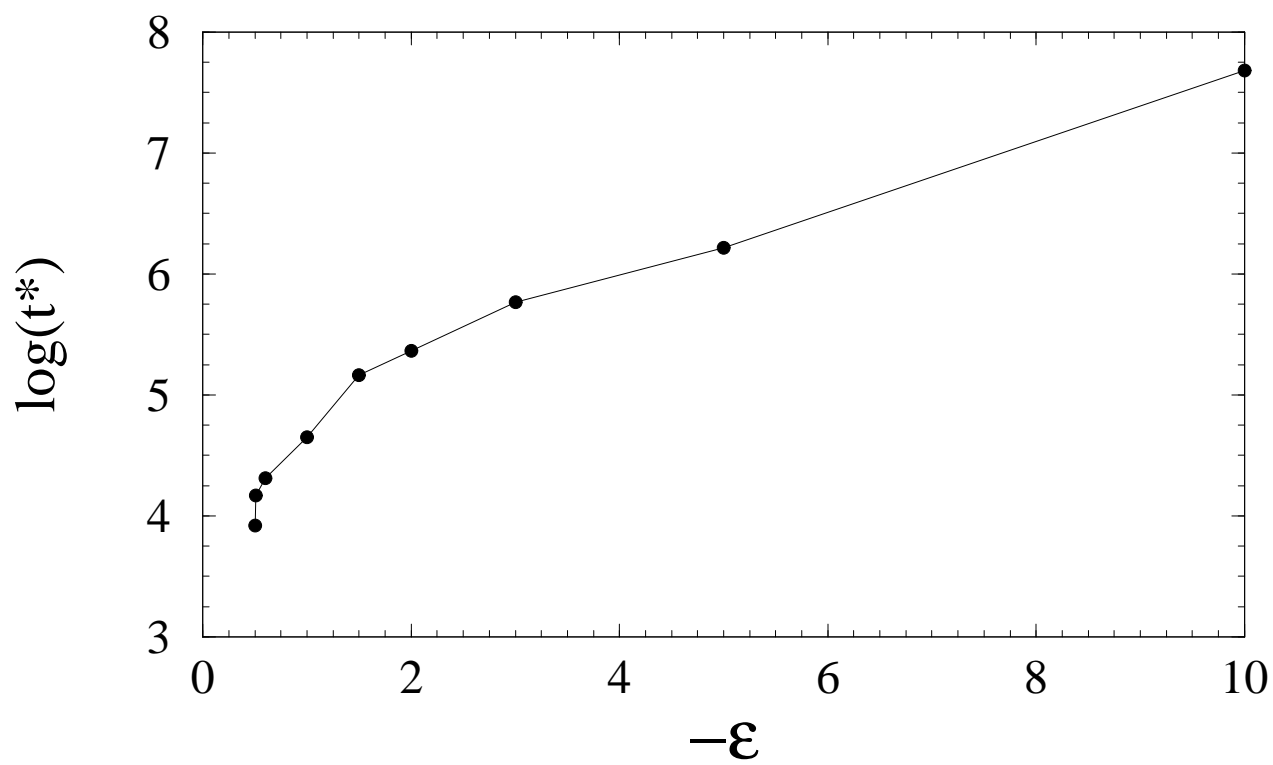
This figure "figure6.gif" is available in "gif" format from:

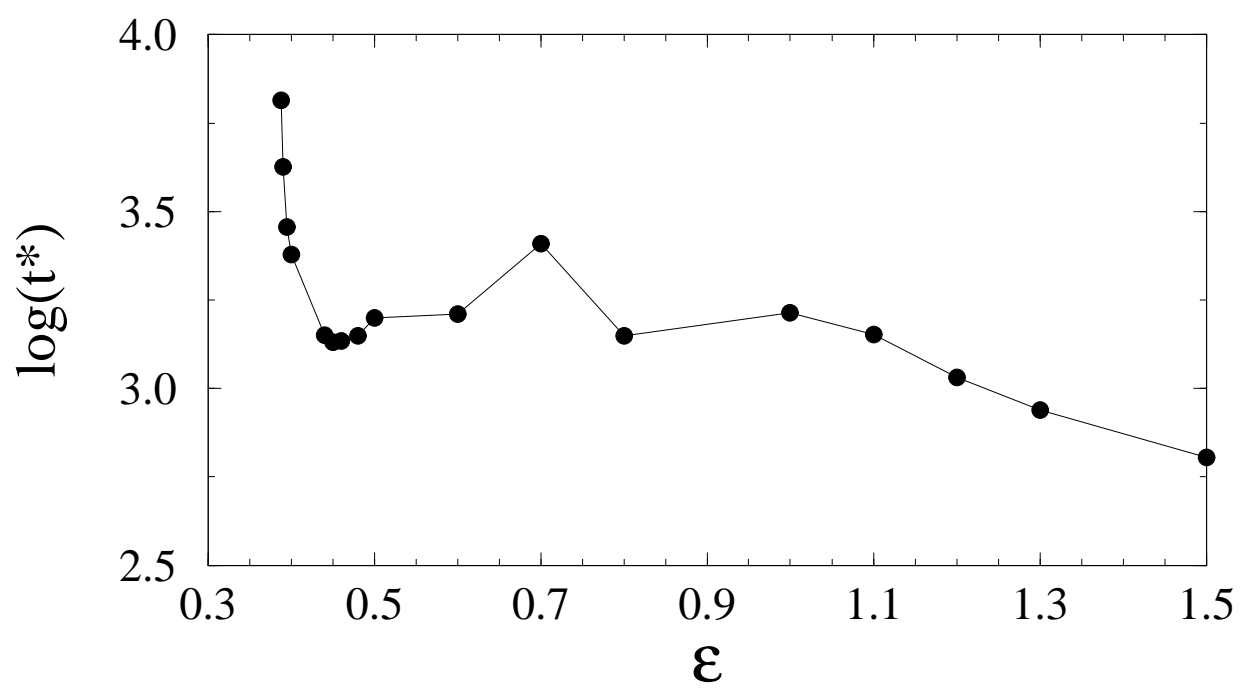
<http://arXiv.org/ps/nlin/0403043v1>



This figure "figure8.gif" is available in "gif" format from:

<http://arXiv.org/ps/nlin/0403043v1>





This figure "figure11.gif" is available in "gif" format from:

<http://arXiv.org/ps/nlin/0403043v1>

This figure "figure12.gif" is available in "gif" format from:

<http://arXiv.org/ps/nlin/0403043v1>

This figure "figure13.gif" is available in "gif" format from:

<http://arXiv.org/ps/nlin/0403043v1>